New Journal of Physics
The open access journal at the forefront of physics

Deutsche Physikalische Gesellschaft DPG IOP Institute of Physics

PAPER

Simulation of quantum magnetism in mixed-spin systems with impurity-doped ion crystals

To cite this article: Peter A Ivanov and Ferdinand Schmidt-Kaler 2011 *New J. Phys.* **13** 125008

New Journal of Physics
The open-access journal for physics

Simulation of quantum magnetism in mixed-spin systems with impurity-doped ion crystals

Peter A Ivanov[1] **and Ferdinand Schmidt-Kaler**
Institut für Physik, Johannes Gutenberg-Universität Mainz,
55099 Mainz, Germany
E-mail: ivanovpe@uni-mainz.de

New Journal of Physics **13** (2011) 125008 (15pp)
Received 26 April 2011
Published 9 December 2011
Online at http://www.njp.org/
doi:10.1088/1367-2630/13/12/125008

Abstract. We propose the realization of linear crystals of cold ions that contain different atomic species for investigating quantum phase transitions and frustration effects in spin systems beyond the commonly considered case of $s = \frac{1}{2}$. Mutual spin–spin interactions between ions can be tailored via the Zeeman effect by applying oscillating magnetic fields with strong gradients. Further, collective vibrational modes in the mixed ion crystal can be used to enhance and to vary the strength of spin–spin interactions and even to switch the nature of the interacting forces from a ferro- to an antiferromagnetic character. We consider the behavior of the effective spin–spin couplings in an ion crystal of spin-1/2 ions doped with high-magnetic-moment ions with spin $S = 3$. We analyze the ground state phase diagram and find regions with different spin orders including ferrimagnetic states. In the most simple nontrivial example, we deal with a linear $\{Ca^+, Mn^+, Ca^+\}$ crystal with spins of $\{\frac{1}{2}, 3, \frac{1}{2}\}$. To demonstrate feasibility with current state-of-the-art experiments, we discuss how quantum phases might be detected using a collective Stern–Gerlach effect of the ion crystal and high-resolution spectroscopy. Here, the state-dependent laser-induced fluorescence of the indicator spin-1/2 ion, of species $^{40}Ca^+$, is used to reveal also the spin state of the simulator spin-3 ions, $^{50}Mn^+$, which does not possess suitable levels for optical excitation and detection.

[1] Author to whom any correspondence should be addressed.

Contents

1. Introduction

Current ion trapping technology has led to rapid progress toward the realization of elementary quantum processors [1, 2]. The ability to control the motional and internal states of the trapped ions with high accuracy allows for the experimental implementation of several textbook models such as quantum simulations of a Dirac equation with the Zitterbewegung and the Klein paradox [3, 4]. On the other hand, the internal states of laser-cooled and trapped ions represent effective spins, which can be made to interact with each other for performing magnetic quantum phase simulations. These interactions may be realized by applying magnetic field gradients [5–10] or by laser light fields [11–15]. In both cases, spin-1/2 ion crystals allow for a detailed investigation of complex quantum phase transitions and magnetic frustrated effects. Preliminary experimental steps in ion crystals have been realized with interacting spins of two $^{25}Mg^{+}$ [16] and up to nine $^{171}Yb^{+}$ ions [15, 17] in a linear configuration. Because of the long-range spin–spin interactions, the larger collections of trapped ions are expected to lead to intriguing and so far unobserved phenomena, such as the formation of super-solids [18] or exotic quantum phases [19], where the specific advantages of the ion crystal are: almost perfect state preparation and readout with single-site addressability, long coherence times and a full tunability of the spin–spin interactions, even for long ranges beyond next-neighbor couplings.

Going beyond spin-1/2 systems and trapping different ion species with spin $S > 1/2$ will allow the study of novel aspects of quantum magnetism in mixed spin chains [20, 21]. Such impurity-doped systems might model effects that are of interest in solid state physics [22, 23]. Our proposal is inspired by the outstanding progress in quantum logic spectroscopy [24, 25], where a single clock ion and a single readout ion are simultaneously confined and coupled through mutual Coulomb repulsion, such that one can transfer the clock ion electronic state to the readout ion for high-fidelity quantum state detection [26]. A different, new type of quantum logic readout technique enables us to propose quantum simulation in *mixed ion crystals*. For the case of interacting neutral atoms, the high magnetic moment of $6\mu_B$ of chromium has led to a wealth of novel effects [27, 28], made possible by the tuning of its spin interactions. ^{50}Mn, with

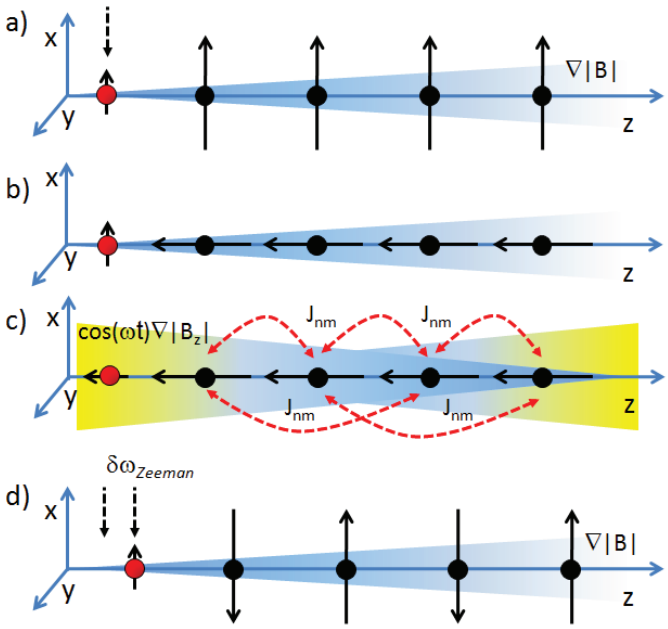

Figure 1. Sketch of the proposed experimental sequence, beginning with (a) the initialization of the spins (indicated by solid arrows) by using the static magnetic gradient field, followed by (b) a radiofrequency (RF) $\pi/2$ pulse on the Mn^+ ions and (c) the creation of spin–spin interactions (red dashed lines) by using an oscillating magnetic gradient field, and finally concluded by (d) a collective spin readout on the auxiliary Ca^+ ion (left red circle) using the position-dependent Stern–Gerlach effect. The shift of the equilibrium position of the auxiliary ion due to the spin-dependent force causes a frequency separation indicated by $\delta\omega_{\mathrm{Zeeman}}$ (see section 4). This leads to a bright or dark state of the Ca^+ ion, which is imaged on a CCD camera via state-dependent fluorescence.

an atomic number that is +1 higher as compared with Cr, features a similar electronic structure and magnetic moment when singly ionized to Mn^+ for being trapped in the ion crystal.

In this paper, we propose an efficient method for the creation of effective spin–spin interactions in ion crystals of spin-1/2 ions doped with different ion species with spin $S = 3$. An oscillating magnetic field gradient [8] can be used to implement coupling between the spin states of both ion species and the collective motional states of the impurity-doped crystal (see figure 1). The advantage of using an oscillating magnetic field instead of a laser field is that it is possible to avoid technical difficulties such as sideband cooling of the many vibrational modes and the necessity to use additional lasers to provide the spin–spin couplings. We show that by a proper choice of the frequencies and direction of the magnetic field gradient, the anisotropic Heisenberg model can be realized with tunable spin–spin couplings [29]. We investigate the particular case of a field gradient applied along the trapping axis such that the spin–spin interactions are described by the transverse Ising model with *single-ion anisotropy*. We consider the ground state phase diagram for a small system consisting of two spin-1/2 ions and one spin-3 ion placed at the center, which is realizable with current ion-trap technology. Due to the complex competition between the spin–spin couplings and the single-ion anisotropy, we are able to distinguish four

regions with different spin orders [15]. We found that for sufficiently strong antiferromagnetic nearest-neighbor coupling, the spin order is *ferrimagnetic* wherein the two different spins are arranged in opposite directions. We show that the ferrimagnetic order can be frustrated due to competing next-nearest-neighbor coupling and the single-ion anisotropy which gives rise to a highly entangled ground state.

It has been shown that the atomic gases in an optical lattice may be used to realize various condensed-matter models with high spin symmetry [21, 30]. The ability to trap ions with large spins at a fixed position [31] and to tune the range and strength of the interactions makes the impurity-doped ion crystal an analogue quantum simulator for quantum magnetism and frustration effects in a mixed spin system [32, 33].

The paper is organized as follows. In section 2, we describe the theoretical background for the implementation of the effective spin–spin interactions in an $(S, s) = (3, \frac{1}{2})$ mixed spin system by using an oscillating magnetic field gradient. In section 3, we provide an analysis of the ground state phase diagram for the transverse Ising Hamiltonian with single-ion anisotropy describing a spin system with two spin-1/2 ions and one spin-3 ion placed at the center. The method for state preparation and readout of the spin states based on frequency addressing of the auxiliary ion is considered in section 4. Finally, in section 5 we give a summary of the results and discuss further and even more complex possibilities of quantum simulation with mixed ion crystals.

2. Theoretical model

We consider a harmonically confined impurity-doped ion crystal with $N - K$ spin-1/2 ions with mass m and K spin-3 ions with mass M. For instance, this is the case of a $^{40}Ca^+$ ion crystal doped with $^{50}Mn^+$ ions, which have $^7S_3$ electronic ground state. If the radial trap frequencies are much larger than the axial trap frequency ($\omega_{x,y} \gg \omega_z$), the ions arrange themselves in a linear configuration along the axial z-axis and occupy equilibrium positions [34]. The axial trap potential is independent of the mass, so that the equilibrium position of the ions is independent of the composition of the ion crystal. A static magnetic field B_0 along the trap axis defines the quantization axis. The spin-1/2 sublevels $|\uparrow\rangle$ and $|\downarrow\rangle$ are Zeeman split by the applied magnetic field with a resonance frequency $\omega_0 = (g_J \mu_B/\hbar) B_0$. Here g_J denotes the Landé g-factor and μ_B is the Bohr magneton. The spin sublevels of spin-3 ions possess seven Zeeman states, which we index as $|m\rangle$ with magnetic quantum number $m = -3, -2, \ldots, +3$ and resonance frequency $\tilde{\omega}_0$. In the case of an ion crystal consisting of $^{40}Ca^+$ ions with electronic ground state $^2S_{1/2}$ doped with $^{50}Mn^+$ ions, the Landé g-factor is $g_J \approx 2$ such that the resonance frequencies ω_0 and $\tilde{\omega}_0$ of both ion species are equal.

2.1. Magnetic field gradient along the z-direction

We assume that the impurity-doped ion crystal interacts collectively with the oscillating magnetic gradient field with frequency ω applied along the z-direction (for simplicity we omit the constant magnetic offset)

$$\vec{B} = \vec{e}_z z B_z \cos \omega t. \tag{1}$$

The Hamiltonian for N ions interacting with the magnetic field is $\hat{H} = \hat{H}_0 + \hat{H}_I$. Here

$$\hat{H}_0 = \frac{\hbar\omega_0}{2}\sum_{j=1}^{N-K}\sigma_j^z + \hbar\omega_0\sum_{k=1}^{K}S_k^z + \hbar\sum_{n=1}^{N}\omega_{n,z}\hat{a}_{n,z}^{\dagger}\hat{a}_{n,z} \tag{2}$$

is the interaction-free Hamiltonian, with σ_j^z being the Pauli matrix for the jth spin-1/2 ion and S_k^z is the spin operator for the kth spin-3 ion with $S_z|m\rangle = m|m\rangle$. $\hat{a}_{n,z}^{\dagger}$ and $\hat{a}_{n,z}$ are, respectively, the creation and annihilation operators of collective phonons along the z-axis with frequency $\omega_{n,z}$. The displacement $\hat{z}_j$ of the jth ion from its equilibrium position can be expressed in terms of this set of operators as $\hat{z}_j = \sum_{n=1}^{N} b_{j,n}^z \Delta z_n(\hat{a}_{n,z}^{\dagger} + \hat{a}_{n,z})$. Here $\Delta z_n(a) = \sqrt{\hbar/2a\omega_{n,z}}$ with $a = m, M$ being the spread of the ground state wave function and $b_{j,n}^z$ $(n = 1, 2, \ldots, N)$ being the normal mode eigenvectors in the z-direction (see appendix) [34, 35]. The interaction between the magnetic dipole moment of the ion species and the magnetic gradient is described by $\hat{H}_I = -\hat{\vec{\mu}}.\vec{B}$. The z-component of the magnetic-dipole moment for the spin-1/2 ion is $\hat{\mu}_z = (\gamma/2)\sigma_z$ and that for a spin-3 is $\hat{\mu}_z = \gamma S_z$ with $\gamma = \mu_B g_J$. Then, we may transform the Hamiltonian in the interaction picture with respect to $\hat{H}_0$ to obtain

$$\begin{aligned}\hat{H}_I^z = &-\hbar\sum_{n=1}^{N}\left(\sum_{j=1}^{N-K}\frac{\Omega_{j,n}^z}{2}\sigma_j^z + \sum_{k=1}^{K}\Omega_{k,n}^z S_k^z\right)\left(\hat{a}_{n,z}^{\dagger}\mathrm{e}^{\mathrm{i}(\omega+\omega_{n,z})t} + \hat{a}_{n,z}\mathrm{e}^{-\mathrm{i}(\omega+\omega_{n,z})t}\right)\\ &-\hbar\sum_{n=1}^{N}\left(\sum_{j=1}^{N-K}\frac{\Omega_{j,n}^z}{2}\sigma_j^z + \sum_{k=1}^{K}\Omega_{k,n}^z S_k^z\right)\left(\hat{a}_{n,z}^{\dagger}\mathrm{e}^{-\mathrm{i}(\omega-\omega_{n,z})t} + \hat{a}_{n,z}\mathrm{e}^{\mathrm{i}(\omega-\omega_{n,z})t}\right).\end{aligned} \tag{3}$$

The function $\Omega_{j,n}^z = b_{j,n}^z \Delta z_n B_z \gamma/2\hbar$ is the Rabi frequency of the jth ion, which quantifies the coupling to the nth vibrational mode. Hence, the oscillating magnetic gradient field mediates a coupling between the internal states of the ions and the external (motional) states of the ion crystal. Indeed, the two terms in the Hamiltonian (3) describe a time-varying spin-dependent displacement with frequencies $(\omega + \omega_{n,z})$ and $(\omega - \omega_{n,z})$. If the frequency ω is not resonant to any vibrational mode and the condition $|\omega_{n,z} - \omega| \gg \Omega_{j,n}^z$ is satisfied for any n, then we can perform time averaging of the rapidly oscillating terms in (3) [36]. Thus, we arrive at the following time-averaged effective Hamiltonian:

$$\hat{H}_{\mathrm{eff}}^z = \hbar\sum_{\substack{j,j'=1\\ j>j'}}^{N-K} J_{j,j'}^{(1,z)}\sigma_j^z\sigma_{j'}^z + \hbar\sum_{\substack{k,k'=1\\ k>k'}}^{K} J_{k,k'}^{(2,z)}S_k^z S_{k'}^z + \hbar\sum_{j=1}^{N-K}\sum_{k=1}^{K} J_{j,k}^{(3,z)}\sigma_j^z S_k^z + \hbar\sum_{k=1}^{K} A_k^z (S_k^z)^2. \tag{4}$$

Therefore, the off-resonant oscillating magnetic gradient creates an effective spin–spin interaction between identical [14, 15] and different ion species in the crystal. The first two terms in (4) quantify the spin–spin coupling between the spin-1/2 ions and the spin-3 ions. The third term in (4) describes the spin–spin coupling between the different ion species. Surprisingly, the adiabatic elimination of the vibrational modes for an ion crystal with $s > 1/2$ ions gives rise to the single-ion anisotropy term $H_{\mathrm{SI}}^{(k)} = A_k^z (S_k^z)^2$, which quantifies the nonlinear Zeeman shift of the spin-3 magnetic sublevels. This term resembles the situation in a solid state, where the single-ion anisotropy describes the coupling between the spins and a crystal field, which is created by the neighboring atoms [37]. In the case of the impurity-doped ion system, this interaction results in an energy preference of the spins $S > \frac{1}{2}$ to align in a particular direction.

For ions with $s = \frac{1}{2}$ the nonlinear Zeeman shift is equal for both magnetic sublevels, and thereby proportional to the unit matrix. The couplings in (4) are given by

$$J^{(1,z)}_{j,j'} = \frac{B_z^2\gamma^2}{8\hbar m}\sum_{n=1}^{N}\frac{b^z_{j,n}b^z_{j',n}}{\omega^2-\omega^2_{n,z}}, \qquad J^{(2,z)}_{k,k'} = \frac{B_z^2\gamma^2}{2\hbar M}\sum_{n=1}^{N}\frac{b^z_{k,n}b^z_{k',n}}{\omega^2-\omega^2_{n,z}},$$

$$J^{(3,z)}_{j,k} = \frac{B_z^2\gamma^2}{4\hbar\sqrt{mM}}\sum_{n=1}^{N}\frac{b^z_{j,n}b^z_{k,n}}{\omega^2-\omega^2_{n,z}}, \qquad A^z_k = \frac{B_z^2\gamma^2}{4\hbar M}\sum_{n=1}^{N}\frac{(b^z_{k,n})^2}{\omega^2-\omega^2_{n,z}}. \tag{5}$$

The main advantage of using an oscillating magnetic field gradient instead of constant is that we may engineer a variety of interactions between the ions. Figure 2 shows the spin–spin couplings and the single-ion anisotropy (5) for a chain of two spin-1/2 ions and one spin-3 ion placed at the center versus the frequency ω. In contrast to having constant magnetic field gradient applied along the trapping axis z wherein the spin couplings can be only ferromagnetic, here the magnitude and sign of the couplings change as ω is varied, which allows the creation of ferromagnetic, antiferromagnetic or frustrated interaction between the ions. The ground state of the Hamiltonian (4) highly depends on the sign of the single-ion anisotropy terms A^z_k. Indeed, for sufficiently large positive single-ion anisotropy ($A^z_k \gg 0$), the spin-3 ions have magnetic quantum number $m = 0$ for the ground state, while in the opposite limit ($|A^z_k| \gg 0$) the spin-3 ground state projection is $m = \pm 3$.

2.2. *Magnetic field along the xyz-direction*

Consider the magnetic gradient applied along the xyz-direction

$$\vec{B}(x, y, z) = \vec{e}_z z B_z \cos\omega t + \vec{e}_x x B_x f(t) - \vec{e}_y y B_y f(t), \tag{6}$$

with $f(t) = (\cos\omega_b t + \cos\omega_r t)$. Such a field can be created in a micro-structured planar ion trap, which contains a central wire loop [9]. The oscillating field in the x–y-plane provides additional coupling $\Omega^q_{j,n} = b^q_{j,n}\Delta q_n B_q\gamma/2\hbar$ ($q = x, y$) between the internal and motional degrees of freedom of the ion crystal. We assume that the frequencies $\omega_b - \omega_0 = \delta$ and $\omega_r - \omega_0 = -\delta$ are tuned to the blue- and red-sideband transitions with detuning $\pm\delta$. Then the x–y gradients induce a spin-dependent displacement with frequencies $(\delta + \omega_{n,q})$ and $(\delta - \omega_{n,q})$ similar to equation (3), where $\omega_{n,q}$ are the vibrational frequencies in the x- and y-directions, respectively (see appendix). After applying an optical rotating-wave approximation (neglecting the terms $\omega_0 + \omega_{b,r}$) and assuming that $|\omega_{n,q} - \delta| \gg \Omega^q_{j,n}$ is fulfilled for any vibrational mode in the x–y-direction, the time-averaged effective Hamiltonian is given by

$$\hat{H}_{\text{eff}} = \hbar\sum_{q=x,y,z}\left\{\sum_{\substack{j,j'=1\\ j>j'}}^{N-K} J^{(1,q)}_{j,j'}\sigma^q_j\sigma^q_{j'} + \sum_{\substack{k,k'=1\\ k>k'}}^{K} J^{(2,q)}_{k,k'}S^q_k S^q_{k'} + \sum_{j=1}^{N-K}\sum_{k=1}^{K} J^{(3,q)}_{j,k}\sigma^q_j S^q_k + \sum_{k=1}^{K} A^q_k (S^q_k)^2\right\}. \tag{7}$$

The spin–spin couplings in the x–y direction are identical in form to (5) by replacing $\omega \to \delta$ and $z \to x, y$. We note that the condition div $\vec{B} = 0$ for the magnetic field in the x–y plane gives rise to a constraint for the magnetic field gradients, $B_x = B_y$. However, this condition does not give the restriction to the spin couplings as long as the trapping frequencies ω_x and ω_y are different, such that in general we have $J^{(x)}_{k,k'} \neq J^{(y)}_{k,k'}$. Hence, the magnetic field (6) creates an anisotropic (XYZ) Heisenberg interaction between the effective spins.

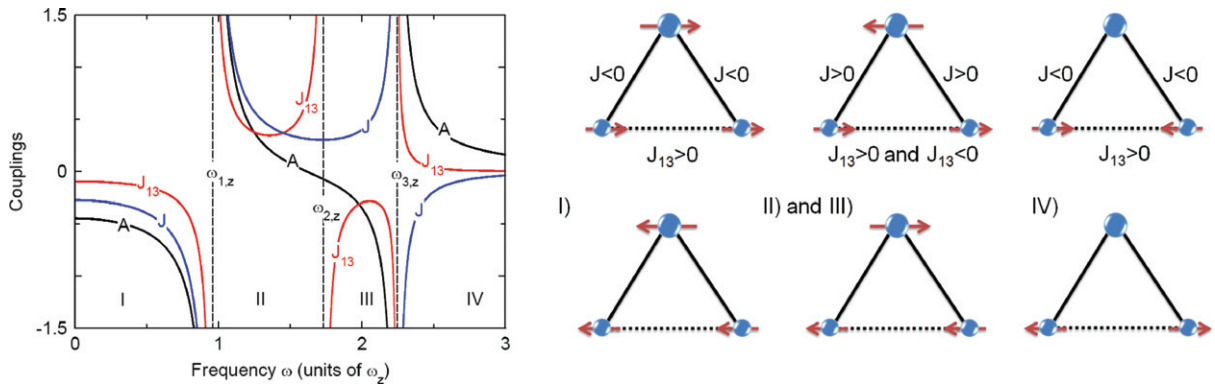

Figure 2. (Left) The nearest neighbor $J_{12} = J_{23} = J$, the next-nearest neighbor J_{13} spin–spin couplings and the single-ion anisotropy A as a function of ω for an ion crystal consisting of two spin-1/2 ions and one spin-3 ion placed at the center (see equation (5)). The couplings J, J_{13} and A are normalized to $\varepsilon = (\Delta z \partial_z \omega_0)^2/(2\omega_z)$, which quantifies the change of the spin resonance frequency ω_0 due to the shift of the equilibrium position of the ion with trap frequency ω_z by an amount equal to the spread of the ground state wavefunction, $\Delta z = \sqrt{\hbar/2m\omega_z}$. (Right) Quantum phases differ in the region (I)–(IV).

3. Transverse Ising model

The quantum transverse Ising Hamiltonian is given by

$$H_{\mathrm{TI}} = H^z_{\mathrm{eff}} - \hbar B^0_x \left\{ \sum_{j=1}^{N-K} \frac{\sigma^x_j}{2} + \sum_{k=1}^{K} S^x_k \right\}. \tag{8}$$

The last term in (8) can be simulated by driving transitions between the ion spin states employing a radiofrequency (RF) field $\vec{B}_0 = \vec{e}_x B_0 \cos \tilde{\omega} t$. Assuming that the resonance condition is fulfilled, i.e. $\tilde{\omega} = \omega_0$ we obtain the effective transverse field $B^0_x = \gamma B_0/2\hbar$.

The simplest nontrivial case is to consider an ion chain with two spin-1/2 ions and one spin-3 ion placed at the center. Such an ordering of ions is consistent with natural behavior, as observed in [31]. When applying an oscillating gradient field, the resulting spin–spin couplings are shown in figure 2 as a function of the drive frequency ω. We may distinguish between four different regions wherein the spin–spin interactions are ferromagnetic, antiferromagnetic or frustrated. The presence of the single-ion anisotropy A in (8) changes substantially the ground state phase diagram compared to the case of spin-1/2 ion chain. In contrast to the spin-1/2 string, the ground state of the mixed $(S, s) = (3, \frac{1}{2})$ spin system can be frustrated due to the complex competition between the spin–spin couplings J and J_{13} and the single-ion anisotropy A.

In region (I) (see figure 2) all interactions are ferromagnetic (J, $J_{13} < 0$) and the resulting ground state of the Hamiltonian (8) as $B^0_x \to 0$ is a coherent superposition of two ferromagnetic states $|\uparrow\uparrow\rangle|3\rangle$ and $|\downarrow\downarrow\rangle|-3\rangle$. Because the single-ion anisotropy is negative ($A < 0$), the ground state energy is minimized for the spin-3 state with magnetic quantum number $m = \pm 3$. The ferromagnetic population $P_{fm,3} = P_{\uparrow\uparrow 3} + P_{\downarrow\downarrow -3}$ as a function of the effective magnetic field and

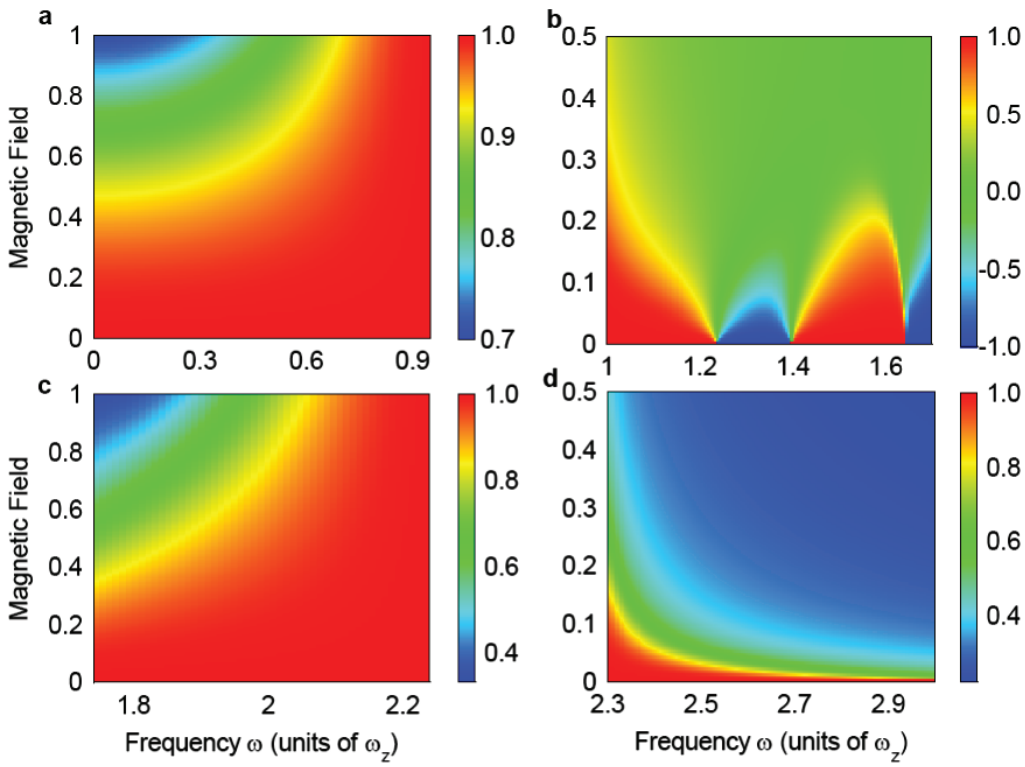

Figure 3. The ground state phase diagram calculated by an exact diagonalization of the Hamiltonian (8). (a) The ferromagnetic population $P_{fm,3}$ as a function of the normalized transverse magnetic field B_x^0/ε and the frequency ω. In region (I), the spin–spin couplings are ferromagnetic J, $J_{13} < 0$ and the single-ion anisotropy is $A < 0$. (b) The population difference $P_{f,1} - P_{f,2} + P_{f,3} - P_{a,3}$ as a function of the normalized transverse magnetic field B_x^0/ε and the frequency ω. In region (II), the spin–spin couplings are antiferromagnetic J, $J_{13} > 0$ and the single-ion anisotropy is $A > 0$. By increasing ω as $B_x^0 \to 0$ the system undergoes the transition $|\psi_{f,1}\rangle \to |\psi_{f,2}\rangle \to |\psi_{f,3}\rangle \to |\psi_{a,3}\rangle$. (c) The ferrimagnetic population $P_{f,3}$ as a function of the normalized transverse magnetic field B_x^0/ε and the frequency ω. In region (III), the spin–spin couplings are $J > 0$, $J_{13} < 0$, respectively, and the single-ion anisotropy is $A < 0$. (d) The antiferromagnetic population $P_{a,0}$ as a function of the normalized transverse magnetic field B_x^0/ε and the frequency ω. In region (IV), the spin–spin couplings are $J < 0$, $J_{13} > 0$, respectively, and the single-ion anisotropy is $A > 0$.

the frequency ω is shown in figure 3(a). In region (II), the spin interactions are antiferromagnetic (J, $J_{13} > 0$). This is the case for ferrimagnetism in which spins of two types interact by nearest-neighbor antiferromagnetic coupling (see figure 3(b)). However, the ferrimagnetic interaction is frustrated due to the competing next-nearest-neighbor antiferromagnetic coupling $J_{13} > 0$, which disturbs the ferrimagnetic order and tends to align the two spins-$\frac{1}{2}$ in an antiferromagnetic state. Additionally, the ferrimagnetic interaction is also frustrated due to the strong positive single-ion anisotropy $A > 0$, which attempts to project the spin-3 state $|m\rangle$ in a quantum number $m = 0$. In the beginning of region (II), $A > 0$ is high but the ferrimagnetic configuration

is still energetically favorable such that the ground state of the Hamiltonian (8) as $B_x^0 \to 0$ becomes a superposition of two ferrimagnetic states $|\psi_{f,1}\rangle = (|\uparrow\uparrow\rangle|-1\rangle + |\downarrow\downarrow\rangle|1\rangle)/\sqrt{2}$, wherein the spins $S = 3$ and $s = \frac{1}{2}$ are aligned anti-parallel to each other. By increasing ω, the single-ion anisotropy A decreases, which allows the quantum number m to increase and the resulting ground state is $|\psi_{2,f}\rangle = (|\uparrow\uparrow\rangle|-2\rangle + |\downarrow\downarrow\rangle|2\rangle)/\sqrt{2}$. For $A/J = 2/3$, which occurs at $\omega \approx 1.24\omega_z$, the ground state for $B_x^0 = 0$ is an entangled superposition of four ferrimagnetic states $|\uparrow\uparrow\rangle|-1\rangle$, $|\downarrow\downarrow\rangle|1\rangle$, $|\uparrow\uparrow\rangle|-2\rangle$ and $|\downarrow\downarrow\rangle|2\rangle$. By decreasing A the ferrimagnetic state $|\psi_{2,f}\rangle$ undergoes a transition to $|\psi_{3,f}\rangle = (|\uparrow\uparrow\rangle|-3\rangle + |\downarrow\downarrow\rangle|3\rangle)/\sqrt{2}$. At the transition point $\omega = 1.4\omega_z$ and $A/J = 0.4$ the resulting ground state for $B_x^0 = 0$ is an entangled superposition of four ferrimagnetic states, $|\uparrow\uparrow\rangle|-2\rangle$, $|\downarrow\downarrow\rangle|2\rangle$, $|\uparrow\uparrow\rangle|-3\rangle$ and $|\downarrow\downarrow\rangle|3\rangle$. For sufficiently high positive J_{13} the ferrimagnetic arrangement is not favorable and the two spin-$\frac{1}{2}$ ions are arranged in an antiferromagnetic state. Hence, the ferrimagnetic configuration is broken and the ground state is $|\psi_{a,3}\rangle = (|\uparrow\downarrow\rangle + |\downarrow\uparrow\rangle)(|3\rangle + |-3\rangle)/2$. At the transition point $\omega \approx 1.65\omega_z$, the ground state of the Hamiltonian (8) is an entangled superposition of six states: two ferrimagnetic states $|\uparrow\uparrow\rangle|-3\rangle$ and $|\downarrow\downarrow\rangle|3\rangle$ and four antiferromagnetic states $|\uparrow\downarrow\rangle|3\rangle$, $|\uparrow\downarrow\rangle|-3\rangle$, $|\downarrow\uparrow\rangle|3\rangle$ and $|\downarrow\uparrow\rangle|-3\rangle$. In region (III), the nearest-neighbor spin coupling is antiferromagnetic ($J > 0$) such that the ferrimagnetic configuration is favorable. In contrast with region (II), no frustration exists because the next-nearest-neighbor coupling is ferromagnetic $J_{13} < 0$ and $A < 0$. In the entire region the ground state is ferrimagnetic $|\psi_{f,3}\rangle$, which minimizes all interactions. In figure 3(c), the ferrimagnetic population $P_{f,3} = P_{\uparrow\uparrow-3} + P_{\downarrow\downarrow 3}$ versus the effective magnetic field and the frequency ω is shown. In region (IV), the single-ion anisotropy is positive ($A > 0$), which causes the spin-3 to be projected into quantum number $m = 0$. Additionally, the next-nearest-neighbor coupling is antiferromagnetic $J_{13} > 0$ and the resulting ground state as $B_x^0 \to 0$ is antiferromagnetic $|\psi_{a,0}\rangle = (|\uparrow\downarrow\rangle + |\downarrow\uparrow\rangle)|0\rangle/\sqrt{2}$. The antiferromagnetic population $P_{a,0} = P_{\uparrow\downarrow 0} + P_{\downarrow\uparrow 0}$ is shown in figure 3(d).

3.1. Towards larger and more complex mixed crystals

By increasing the number of ions the spin–spin interactions become more complex and consequently the new ground states exhibit a variety of spin orders. In alternating mixed-spin chains we can find regions in which the nearest-neighbor interactions are antiferromagnetic with ferrimagnetic ground states (see figure 4). Such antiferromagnetic mixed-spin chains have been proposed as a model for describing certain molecular-based magnets of experimental interest [38]. Moreover, one of the most studied topics in alternating mixed-spin chains is the appearance of a plateau in the magnetization curve [33, 39–41]. It has been shown that the formation of these plateaux depends strongly on the competing interactions and single-ion anisotropy. Thus, the proposed ion trap-based simulator of quantum magnetism in the mixed-spin system will allow for detailed studies of such phenomena.

4. Preparation and spin readout

In order to prepare the initial state of the Hamiltonian

$$\hat{H}_{\mathrm{TI}}^0 = -\hbar B_x^0 \left\{ \frac{\sigma_1^x}{2} + S_2^x + \frac{\sigma_3^x}{2} \right\} \tag{9}$$

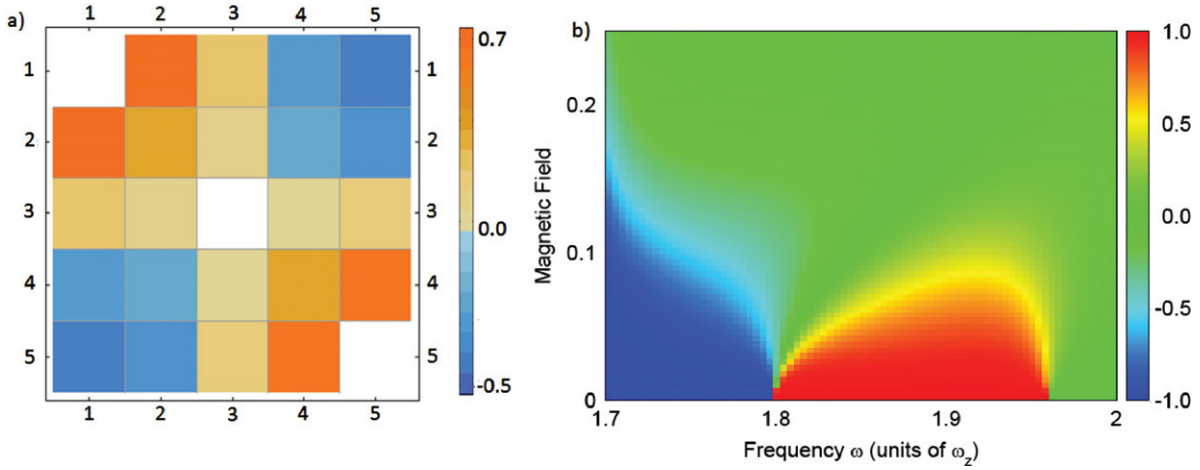

Figure 4. (a). The spin–spin couplings and single-ion anisotropy in an alternating mixed-spin chain $\{\frac{1}{2}, 3, \frac{1}{2}, 3, \frac{1}{2}\}$ consisting of three spin-1/2 ions and two spin-3 ions. All couplings are normalized to ε. The frequency of the oscillating magnetic field is set to $\omega = 1.8\omega_z$. The nearest-neighbor couplings are antiferromagnetic. Similar antiferromagnetic behavior is observed in larger alternating odd number ion crystals. (b) Because of the antiferromagnetic nearest-neighbor interactions, the different spins are aligned anti-parallel to each other and the resulting ground state as $B_x^0/\varepsilon \to 0$ is ferrimagnetic $|\psi_{f,2}\rangle = (|\uparrow\uparrow\rangle|-2,-2\rangle + |\downarrow\downarrow\rangle|2,2\rangle)/\sqrt{2}$ or $|\psi_{f,3}\rangle = (|\uparrow\uparrow\rangle|-3,-3\rangle + |\downarrow\downarrow\rangle|3,3\rangle)/\sqrt{2}$. The figure shows the population difference $P_{f,3} - P_{f,2}$ as a function of ω and B_x^0/ε.

and to readout the final state after the adiabatic ramping of the spin couplings, we can apply a static magnetic field gradient $\vec{B} = \vec{B}_0 + bz\vec{e}_z$ along the trapping axis z which shifts the resonance frequencies of transitions between Zeeman states (see figure 5(a) and the general scheme in figure 1). Due to the spatial variation of the magnetic field, the spin states exhibit site-specific resonance frequencies, $\omega_0' = \omega_0 + \gamma bz/\hbar$. Due to the applied gradient field, the equilibrium position of each of the ions is shifted depending on the spin states of the other ions in the linear crystal. Indeed, the total force that acts on the magnetic dipole moment of spin-1/2 ions along the trapping axis z is $F_1 = F_z^{(2)} + F_z^{(3)}$, where $F_z^{(2)} = \hbar\partial_z\omega\langle S_z\rangle$ and $F_z^{(3)} = (\hbar/2)\partial_z\omega\langle\sigma_z\rangle$ are forces associated with the spins $\hbar S_z$ and $(\hbar/2)\sigma_z$ in a magnetic field $\vec{B}$ and $\langle\rangle$ indicates the expectation value [5]. The spin-dependent force shifts the equilibrium position by an amount $d_z = (F_z^{(2)} + F_z^{(3)})/(m\omega_z^2)$. Consequently, the spin resonance frequency is changed from ω_1 to ω_1', with $\omega_1' = \omega_1 + \gamma bd_z/\hbar$ (see figure 5(b)). The frequency separation $\delta\omega_{\text{Zeeman}} = |\omega_1' - \omega_1|$ between the two spin resonances of spin-1/2 ion is given by

$$\delta\omega_{\text{Zeeman}} = \frac{\mu_{\text{B}} g_J b}{\hbar}|d_z|. \tag{10}$$

Assuming a high but realistic magnetic gradient of $b = 20\,\text{T}\,\text{m}^{-1}$ [10] and an axial trap frequency of $\omega_z = 2\pi \times 100\,\text{kHz}$, the shift from the equilibrium position of a spin-1/2 ion corresponding to the state $|m = 3\rangle_2|\uparrow\rangle_3$ is $d_z \approx 50\,\text{nm}$, which gives rise to frequency separation (10) of $\delta\omega_{\text{Zeeman}} \approx 174\,\text{kHz}$. Note that much smaller frequency shifts are easily

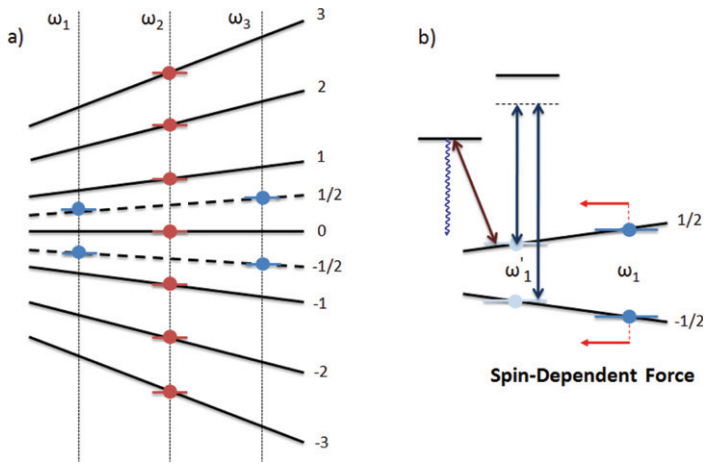

Figure 5. (a) In the presence of static magnetic field gradient, the Zeeman shift of the spin states is different for each ion. (b) The ion equilibrium position is shifted due to the spin-dependent force acting on the magnetic dipole moment. The direction and magnitude of the displacement depend on the spin states of the other ions. Thus, the spin resonance frequency will change from ω_1 to ω_1'. By scanning the frequency of the applied laser light, the spin transition comes into resonance and consequently the ion scatters light.

resolved on a narrow Raman or quadrupole transition, such that in a final step the observation of laser-induced fluorescence allows one to determine the spin states. The experimental sequence is started by preparing the two spin-1/2 ions in a state $|\downarrow\downarrow\rangle|\Psi_S\rangle$, where $|\Psi_S\rangle$ is a still unknown state of the spin-3 ion. Additionally, we may trap an auxiliary ion initially prepared by optical pumping in the state $|\downarrow\rangle_a$ which can be used to readout the spin states of the remaining three ions. In the second step we switch on the static magnetic gradient, which creates the spin-dependent force. Next, we expose the auxiliary ion to laser light with frequency ω_1', which drives the transition $|\downarrow\rangle_a \leftrightarrow |\uparrow\rangle_a$ only if the state of the spin-3 ion is $|m=-3\rangle$. If the auxiliary ion does not scatter light we have to discard the measurement and restart. If we observe fluorescence, then the state of the spin-3 ion is measured in $|-3\rangle$ and results, after performing a $\pi/2$ rotation along the y-axis, in the desired ground state $|\Psi_0\rangle$ of Hamiltonian (9)

$$|\Psi_0\rangle = \mathrm{e}^{-\mathrm{i}\frac{\pi}{4}\sigma_1^y}\mathrm{e}^{-\mathrm{i}\frac{\pi}{2}S_2^y}\mathrm{e}^{-\mathrm{i}\frac{\pi}{4}\sigma_3^y}\,|\downarrow\downarrow\rangle\,|-3\rangle. \tag{11}$$

In the same way, the probability observable $P_{s_1,s_3,m}$ for the state $|s_1 s_3\rangle|m\rangle$ can be determined. By scanning the laser frequency, the auxiliary spin-1/2 ion comes into resonance and consequently scatters light. The auxiliary resonance frequency is defined depending on the spin states of the other three ions. The readout method cannot be applied directly to a general collective spin state with more than one spin-3 ion. For example, in a mixed-spin system with two spin-1/2 ions and two spin-3 ions, the states $|\uparrow\uparrow\rangle|m,-m\rangle$ and $|\uparrow\uparrow\rangle|-m,m\rangle$ create equal amounts of displacement to the equilibrium position of the auxiliary ion, such that both states are indistinguishable. For these more general cases, the state detection problem can be solved by (i) applying a spatially varying magnetic field gradient with $\partial^2 B/\partial z^2 \neq 0$, which allows one to distinguish the spin states due to the position dependence of the force, or

(ii) separating the entire ion crystal into smaller sub-crystals and transporting them into magnetic gradient detection zones [42, 43], which is a promising solution, especially for segmented micro traps [9]. The very precise measurement of the position wave function of an ion, which was a key element in experiments that demonstrated the quantum random walk [44], was also used in other ion trap experiments with single ions and relies on the light ion interaction in either Raman [45] or bichromatic light fields [3, 44]. These methods can determine the wave packet position to an accuracy of a few per cent of the ground state wavepacket extension Δz_m, but for an application here one would need to lock the laser light phases for position determination with respect to the initialization RF pulses on the ions, which has not been experimentally realized so far.

5. Conclusion and outlook

We have proposed a method for the creation and manipulation of the spin–spin interactions in spin-1/2 ion crystals doped with high-magnetic-moment ions with spin $S = 3$. It is shown that by tuning the frequency and direction of oscillating magnetic field gradients, various fundamental models in quantum magnetism of mixed-spin systems can be realized. Because of the competing long-range spin–spin couplings, the spin orders are extremely numerous even for spin systems consisting of a small number of ions. We have proposed a technique for spin preparation and readout based on the frequency addressing of an indicator spin-1/2 ion in the presence of a spatially varying magnetic field.

In future, we will investigate the decoherence properties of such states and how the quantum simulation is affected by typical noise sources in an ion trap experiment. As the different quantum states are affected very differently by the expected dominating source of noise, the ambient magnetic field fluctuations, we expect that states in decoherence-free subspaces, such as for example $|\psi_{f,1}\rangle = (|\uparrow\uparrow\rangle|-1\rangle + |\downarrow\downarrow\rangle|1\rangle)/\sqrt{2}$, or $|\psi_{a,3}\rangle = (|\uparrow\downarrow\rangle + |\downarrow\uparrow\rangle)(|3\rangle + |-3\rangle)/2$ with zero effective magnetic moment will be preferred. A second future research theme is the combination of spin-dependent forces by magnetic gradients using sophisticated control of multiple segments in a micro trap [9, 46] which form the axial potential for the confinement of the ion crystal in the z-direction. As this potential may be shaped in non-trivial, non-harmonic ways and even with multiple potential wells [47, 48], the interspatial distances in the ion crystal become free parameters instead of being given by the Coulomb repulsion in an overall harmonic potential. Here, it was shown that $2 \times N$ cluster states can be generated [49] as a resource for one-way quantum computing.

Acknowledgment

This work was supported the Bulgarian NSF through numbers VU-I-301/07, D002-90/08 and the German Science Foundation within the SFB-TRR49.

Appendix. Calculation of the eigenfrequencies and eigenvectors of the impurity-doped ion crystal

In order to determine the spin–spin interactions we need to calculate the eigenfrequencies and eigenvectors of the impurity-doped ion crystal. The potential energy of a collection of $N - K$

ions with mass m and K ions with mass M is

$$V = \frac{m\omega_z(m)^2}{2}\sum_{j=1}^{N-K} z_j^2 + \frac{m\omega_r(m)^2}{2}\sum_{j=1}^{N-K}(x_j^2+y_j^2) + \frac{M\omega_z(M)^2}{2}\sum_{k=1}^{K} z_k^2 + \frac{M\omega_r(M)^2}{2}\sum_{k=1}^{K}(x_k^2+y_k^2)$$
$$+\frac{e^2}{8\pi\varepsilon_0}\sum_{\substack{j,k=1\\ j\neq k}}^{N}\frac{1}{\sqrt{(x_j-x_k)^2+(y_j-y_k)^2+(z_j-z_k)^2}}, \tag{A.1}$$

where for simplicity of the notation we assume that the trapping confinements in the radial x–y-direction are equal, $\omega_x = \omega_y = \omega_r$. Here $\omega_z(m) \sim m^{-1/2}$ and $\omega_z(M) \sim M^{-1/2}$ are, respectively, the axial trap frequency for an ion with mass m and M. The radial oscillation frequency $\omega_r^0(a) \sim a^{-1}$ with $a = m, M$ is reduced by the axial trap frequency according to

$$\omega_r(a) = \omega_r^0(a)\left(1 - \frac{\omega_z(a)^2}{2\omega_r^0(a)^2}\right)^{1/2}, \tag{A.2}$$

in lowest-order approximation [50]. For small displacements the motional degrees of freedom in x-, y- and z-directions are decoupled. The Hessian matrices A_{ij} and B_{ij} that describe the small oscillation of the ions around their equilibrium position in the axial z, and respectively, x–y-directions are given by

$$A_{ij} = \begin{cases} 1 + 2\displaystyle\sum_{\substack{j=1\\ j\neq p}}^{N}\frac{1}{|u_j - u_p|^3} & (i = j),\\ \dfrac{-2}{|u_i - u_j|^3} & (i \neq j), \end{cases} \tag{A.3}$$

$$B_{ij} = \begin{cases} 1 - \dfrac{\alpha^2}{2} - \alpha^2\displaystyle\sum_{\substack{j=1\\ j\neq p}}^{N}\frac{1}{|u_j - u_p|^3} & (i = j \neq j_M),\\ \dfrac{1}{\mu} - \dfrac{\alpha^2}{2} - \alpha^2\displaystyle\sum_{\substack{j=1\\ j\neq p}}^{N}\frac{1}{|u_j - u_p|^3} & (i = j = j_M),\\ \dfrac{\alpha^2}{|u_i - u_j|^3} & (i \neq j). \end{cases} \tag{A.4}$$

Here we have introduced the mass ratio $\mu = M/m$ and anisotropy parameter $\alpha = \omega_z(m)/\omega_r^0(m)$ with u_j being the dimensionless equilibrium position of the jth ion. In the above expressions, the index j_M denotes the position of the jth ion with mass M. The eigenfrequencies $\omega_{z,n} = \omega_z(m)\sqrt{\lambda_n}$ and eigenvectors $\mathbf{b}_n^z$ $(n = 1, 2, \ldots, N)$ in the z-direction are given by the diagonalization of the following matrix:

$$\tilde{A}_{ij} = \begin{cases} A_{ij} & (i = j \neq j_M),\\ A_{ij}/\mu & (i = j = j_M),\\ A_{ij} & (i \neq j \neq j_M),\\ A_{ij}/\sqrt{\mu} & (i \text{ or } j = j_M,\ i \neq j),\\ A_{ij}/\mu & (i_M \neq j_M), \end{cases} \tag{A.5}$$

such that $\sum_{j=1}^{N} \tilde{A}_{ij} b_{j,n}^{z} = \lambda_n b_{i,n}^{z}$. In the same way the eigenfrequencies $\omega_{q,n} = \omega_{\mathrm{r}}^{0}(m)\sqrt{\gamma_n}$ and eigenvectors $\mathbf{b}_n^q$ $(q = x, y)$ in the radial direction are obtained by the diagonalization of the following matrix:

$$\tilde{B}_{ij} = \begin{cases} B_{ij} & (i = j \neq j_M), \\ B_{ij}/\mu & (i = j = j_M), \\ B_{ij} & (i \neq j \neq j_M), \\ B_{ij}/\sqrt{\mu} & (i \text{ or } j = j_M,\ i \neq j), \\ B_{ij}/\mu & (i_M \neq j_M), \end{cases} \tag{A.6}$$

with $\sum_{j=1}^{N} \tilde{B}_{ij} b_{j,n}^{q} = \gamma_n b_{i,n}^{q}$.

References

[1] Blatt R and Wineland D J 2008 *Nature* **453** 1008
[2] Häffner H, Roos C F and Blatt R 2008 *Phys. Rep.* **469** 155
[3] Gerritsma R, Kirchmair G, Zähringer F, Solano E, Blatt R and Roos C F 2010 *Nature* **463** 68
[4] Gerritsma R, Lanyon B P, Kirchmair G, Zähringer F, Hempel C, Casanova J, Carcia-Ripoll J J, Solano E, Blatt R and Roos C F 2011 *Phys. Rev. Lett.* **106** 060503
[5] Johanning M, Varon A F and Wunderlich C 2009 *J. Phys. B: At. Mol. Opt. Phys.* **42** 154009
[6] Wunderlich C 2002 *Laser Physics at the Limit* ed H Figger, D Meschede and C Zimmermann (Berlin: Springer)
[7] Mintert F and Wunderlich Ch 2001 *Phys. Rev. Lett.* **87** 257904
[8] Ospelkaus C, Langer C E, Amini J M, Brown K R, Leibfried D and Wineland D J 2008 *Phys. Rev. Lett.* **101** 090502
[9] Welzel J, Bautista-Salvador A, Abarbanel C, Wineman-Fisher V, Wunderlich C, Folman F and Schmidt-Kaler F 2011 *Eur. Phys. J.* D **65** 285–97
[10] Ospelkaus C, Warring U, Colombe Y, Brown K R, Amini J M, Leibfried D and Wineland D J 2011 *Nature* **476** 181
[11] Porras D and Cirac J I 2004 *Phys. Rev. Lett.* **92** 207901
[12] Deng X-L, Porras D and Cirac J I 2005 *Phys. Rev.* A **72** 063407
[13] Kim K, Chang M-S, Islam R, Korenblit S, Duan L-M and Monroe C 2009 *Phys. Rev. Lett.* **103** 120502
[14] Islam R *et al* 2011 *Nature Commun.* **2** 377
[15] Lin G-D, Monroe C and Duan L-M 2011 *Phys. Rev. Lett.* **106** 230402
[16] Friedenauer A, Schmitz H, Glueckert J, Porras D and Schaetz T 2008 *Nature Phys.* **4** 757
[17] Kim K, Chang M-S, Korenblit S, Islam R, Edwards E E, Freericks J K, Lin G-D, Duan L-M and Monroe C 2010 *Nature* **465** 590
Edwards E E, Korenblit S, Kim K, Islam R, Chang M-S, Freericks J K, Lin G-D, Duan L-M and Monroe C 2010 *Phys. Rev.* B **82** 060412
[18] Hauke P, Cucchietti F M, Müller-Hermes A, Banuls M-C, Cirac J I and Lewenstein M 2010 *New J. Phys.* **12** 113037
[19] Bermudez A, Porras D and Martin-Delgado M A 2009 *Phys. Rev.* A **79** 060303
[20] Balents L 2010 *Nature* **464** 199
[21] Gorshkov A V, Hermele M, Gurarie V, Xu C, Julienne P S, Ye J, Zoller P, Demler E, Lukin M D and Rey A M 2010 *Nature Phys.* **6** 289
[22] Eggert S, Syljusen O F, Anfuso F and Andres M 2007 *Phys. Rev. Lett.* **99** 097204
[23] Metavitsiadis A 2011 *Phys. Rev.* B **83** 054409
[24] Rosenband T *et al* 2008 *Science* **319** 1808

[25] Chou C W, Hume D B, Thorpe M J, Wineland D J and Rosenband T 2011 *Phys. Rev. Lett.* **106** 160801
[26] Rosenband T *et al* 2007 *Phys. Rev. Lett.* **98** 220801
[27] Lahaye T, Koch T, Frohlich B, Fattori M, Metz J, Griesmaier A, Giovanazzi S and Pfau T 2007 *Nature* **448** 672
[28] Metz J, Lahaye T, Frohlich B, Griesmaier A, Pfau T, Saito H, Kawaguchi Y and Ueda M 2009 *New J. Phys.* **11** 055032
[29] Johanning M, Braun A, Timoney N, Elman V, Neuhauser W and Wunderlich Chr 2009 *Phys. Rev. Lett.* **102** 073004
[30] Taie S, Takasu Y, Sugawa S, Yamazaki R, Tsujimoto T, Murakami R and Takahashi Y 2010 *Phys. Rev. Lett.* **105** 190401
[31] Jost J D, Home J P, Amini J M, Hanneke D, Ozeri R, Langer C, Bollinger J J, Leibfried D and Wineland D J 2009 *Nature* **459** 683
[32] Haldane F D M 1983 *Phys. Rev. Lett.* **50** 1153
[33] Sakai T and Yamamoto S 1999 *Phys. Rev.* B **60** 4053
[34] James D F V 1998 *Appl. Phys.* B **66** 181
[35] Kielpinski D, King B E, Myatt C J, Sackett C A, Turchette Q A, Itano W M, Monroe C, Wineland D J and Zurek W H 2000 *Phys. Rev.* A **61** 032310
[36] James D F V and Jerke J 2007 *Can. J. Phys.* **85** 625–32
[37] Norberto Majlis 2000 *The Quantum Theory of Magnetism* (Singapore: World Scientific)
[38] Willem J, Bos G, Colin C V and Palstra T T M 2008 *Phys. Rev.* B **78** 094416
[39] Sakai T and Okamoto K 2002 *Phys. Rev.* B **65** 214403
[40] Yamamoto S, Brehmer S and Miseska J-J 1998 *Phys. Rev.* B **57** 13610
[41] Oshikawa M, Yamanaka M and Affleck I 1997 *Phys. Rev. Lett.* **78** 1984
[42] Walther A, Poschinger U G, Ziesel F, Hettrich M, Wiens A, Welzel J and Schmidt-Kaler F 2011 *Phys. Rev.* A **83** 062329
[43] Huber G, Ziesel F, Poschinger U G, Singer K and Schmidt-Kaler F 2010 *Appl. Phys.* B **100** 725
[44] Zähringer F, Kirchmair G, Gerritsma R, Solano E, Blatt R and Roos C F 2010 *Phys. Rev. Lett.* **104** 100503
[45] Poschinger U G, Walther A, Singer K and Schmidt-Kaler F 2010 *Phys. Rev. Lett.* **105** 263602
[46] Schulz S, Poschinger U G, Ziesel F and Schmidt-Kaler F 2008 *New J. Phys.* **10** 045007
[47] Harlander M, Lechner R, Brownnutt M, Blatt R and Hänsel W 2011 *Nature* **471** 200
[48] Brown K R, Ospelkaus C, Colombe Y, Wilson A C, Leibfried D and Wineland D J 2011 *Nature* **471** 196
[49] Wunderlich H, Wunderlich C, Singer K and Schmidt-Kaler F 2009 *Phys. Rev.* A **79** 052324
[50] Singer K, Poschinger U, Murphy M, Ivanov P, Ziesel F, Calarco T and Schmidt-Kaler F 2010 *Rev. Mod. Phys.* **82** 2609